Proceedings of 20th International Congress on Acoustics, ICA 2010

23–27 August 2010, Sydney, Australia

The effect of a solid boundary on the dynamics of a small group of ultrasound driven microbubbles

Michael Li (1), Fatimah Dzaharudin (1), Richard Manasseh (1), Andrew Ooi (1)

(1) Department of Mechanical & Engineeing, University of Melbourne, VIC 3010 Melbourne, Australia

PACS: 43.25.Ts, 43.25.Yw, 43.35.Ei

ABSTRACT

The dynamical behaviour of a small cluster of microbubbles subjected to ultrasound near a solid boundary is investigated. An equation for radial oscillation for bubbles near a plane rigid wall is derived using method of images and solved numerically for a given set of ultrasound parameters. In this paper, it is assumed that all bubbles in the system have the same equilibrium radius and are equidistant from one another and from the solid boundary. With the current mathematical model, it is demonstrated that the presence of a solid wall has a significant effect on the bifurcation structure and the route to chaos of the bubble system. As separation distance between microbubbles and solid boundary is decreased, the bubble system is more likely to exhibit chaos and chaotic behaviour occurs at lower pressure amplitude. Furthermore, the maximum amplitude of the bubble oscillations near solid wall is shown to be related to the number of dominant frequencies in the response of the bubble system. Smaller oscillation amplitude is associated bubble response with smaller number of frequencies while chaotic bubble oscillations will lead to larger oscillation amplitude.

INTRODUCTION

The application of ultrasound driven microbubbles in biomedical acoustics and the possibility of using these microbubbles for targeted drug delivery and gene therapy has inspired numerous studies on the dynamics of microbubbles [1–3]. Keller and Miksis derived an equation based on the classical Rayleigh-Plesset equation [4], and this equation was modified by Parlitz et al. [5], resulting in a model that well describes the oscillations of an isolated bubble at high forcing pressure amplitudes and the behaviour of a bubble during cavitation.

In practice, it is extremely rare for a single bubble to exist in isolation. There are usually other bubbles nearby and it is very likely that they would influence the behaviour of the whole bubble system. Thus, it is important to be able to understand the effects of the coupling interactions between bubbles. Ooi and Manasseh [6] and Chong et al. [7] have performed numerical simulations to investigate the effects of coupling on the dynamics of microbubbles, under the assumptions that all bubbles are equidistant from one another and that each bubble is subject to the same external driving pressure, thus reducing the complexity of the system of ordinary differential equations (ODEs) to be solved. Chong et al. [7], along with other studies such as that of MacDonald and Gomatam [8], also studied the bifurcation characteristics of microbubbles within a bubble system and the effect of coupling on the route to chaos of a small cluster of microbubbles.

In order to expand on the current understanding of the dynamics of microbubbles for use in biomedical applications, it is important to be able to predict the behaviour of microbubbles that are close to a boundary. The study of linearized bubble behaviour for large bubbles (mm sized) close to a planar wall has been conducted by Payne et al [9] and Illesinghe et al [10]. In the nonlinear regime, many studies on the dynamics of bubbles near a solid boundary have concentrated on the cavitation damage caused by the jets formed on bubble collapse (for example [11–14]). These are extreme behaviours brought about by high amplitude forcing of the external pressure field. In this paper, we will concentrate on examining the nonlinear behaviour of small bubbles (μm sized) close to walls. But we will limit our scope to the parameter space (i.e. smaller pressure amplitude) where the microbubbles do not undergo collapse and remain spherical in shape. Similar studies have been carried out by Shima and Tomita [15] and Shima and Fujiwara [16] where they investigated the behaviour of one and two spherical bubbles respectively near a solid boundary in the absence of an external driving pressure field.

The main purpose of this study is to numerically investigate the effect of a plane solid boundary on the dynamics of a small group of ultrasound driven microbubbles. The bifurcation characteristics of such a system will also be explored, since the chaotic dynamics of a system of bubbles is related to the inertial cavitation of the bubbles [17]. The study will be limited to cases where all bubbles in a system have the same equilibrium radius and are equidistant from one another and from the solid boundary. Due to the symmetry of this arrangement, the bubbles all exhibit the same dynamical behaviour. The results obtained from this idealised scenario will hopefully lay the foundations for the study of more realistic microbubble systems in the vicinity of a solid boundary.

THEORY

Consider the following equation of Keller-Miksis-Parlitz form with coupling terms [5; 18] for a cluster of microbubbles in a slightly compressible liquid as used by [7]:

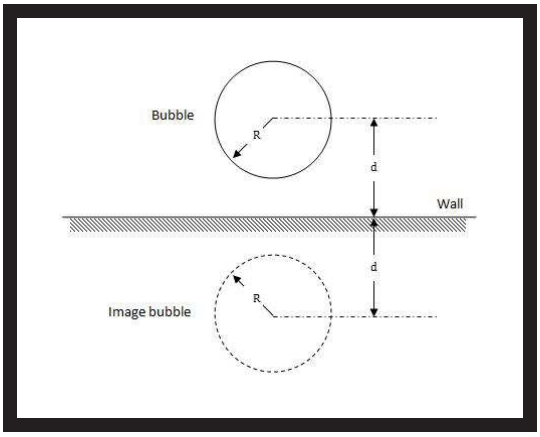

!h

Figure 1: Schematic diagram of a single bubble close to a solid boundary and its image bubble

$$\ddot{R}_i = \frac{1}{\left(1-\frac{\dot{R}_i}{c}\right)R_i + \frac{4\mu}{\rho c}}\left[-\frac{\dot{R}_i^2}{2}\left(3-\frac{\dot{R}_i}{c}\right)\right.$$
$$+\left(1+(1-3\kappa)\frac{\dot{R}_i}{c}\right)\left(\frac{P_0-P_v}{\rho}+\frac{2\sigma}{\rho R_{0i}}\right)\left(\frac{R_{0i}}{R_i}\right)^{3\kappa}$$
$$-\frac{2\sigma}{\rho R_i}-\frac{4\mu\dot{R}_i}{\rho R_i}-\sum_{j\neq i}^{N_{bub}}\frac{1}{s_{ij}}\left(R_j^2\ddot{R}_j+2R_j\dot{R}_j^2\right) \quad (1)$$
$$-\left(1+\frac{\dot{R}_i}{c}\right)\frac{P_0-P_v+\alpha\sin(2\pi f_{ext}t)}{\rho}$$
$$\left.-\frac{2\pi f_{ext}R_i\alpha}{\rho c}\cos(2\pi f_{ext}t)\right]$$

where R_i is the instantaneous bubble radius of bubble i, R_{0i} is the equilibrium bubble radius of bubble i, s_{ij} is the distance between bubbles i and j, μ is the dynamic viscosity of the liquid, ρ is the density of the liquid, κ is the polytropic exponent for the bubble gas, c is the speed of sound in air, σ is the surface tension of the bubble surface, α is the amplitude of the acoustic driving pressure, f_{ext} is the driving frequency and N_{bub} is the number of bubbles. For all simulations in this report, $\mu = 0.001$ kg m^{-1}s^{-1}, $\kappa = 1.33$, $c = 1484$ m s^{-1}, $\sigma = 0.0725$ N m^{-1}, $P_v = 2330$ Pa and $P_0 = 100,000$ Pa. These are accepted values for bubbles in water at 20°C [4].

To derive the equations of motion for a bubble near a solid boundary, the image bubble technique will be used. Other investigators (see [15; 19]) have shown that this methodology gives results that is in good agreement with experimental results. It is assumed that the wall acts as a mirror for each bubble, so that it behaves as though there is an identical "image bubble" the same distance from the wall on the other side of the wall with the same dynamical behaviour (see Fig. 1). Thus we can use Eq. (1) to model each of the bubbles near the solid boundary. Using the image bubble theory, the governing equation for a single bubble close to a wall is given by

$$\ddot{R} = \frac{1}{\left(1-\frac{\dot{R}}{c}\right)R + \frac{4\mu}{\rho c}+\frac{1}{2d}R^2}\left[-\frac{\dot{R}^2}{2}\left(3-\frac{\dot{R}}{c}\right)\right.$$
$$+\left(1+(1-3\kappa)\frac{\dot{R}}{c}\right)\left(\frac{P_0-P_v}{\rho}+\frac{2\sigma}{\rho R_0}\right)\left(\frac{R_0}{R}\right)^{3\kappa}$$
$$-\frac{2\sigma}{\rho R}-\frac{4\mu\dot{R}}{\rho R}-\frac{1}{d}R\dot{R}^2 \quad (2)$$
$$-\left(1+\frac{\dot{R}}{c}\right)\frac{P_0-P_v+\alpha\sin(2\pi f_{ext}t)}{\rho}$$
$$\left.-\frac{2\pi f_{ext}R\alpha}{\rho c}\cos(2\pi f_{ext}t)\right].$$

It is assumed here, amongst the other assumptions used in the derivation of Eq. (1) by previous studies, that all the bubbles remain spherical throughout their motion. This assumption is still a valid approximation even for non-spherical bubbles. Klaseboer and Khoo [20] have shown that non-spherical bubbles can be modelled as spherical bubbles with an equivalent radius that give the same bubble volume.

When there are more than one bubbles in the system, every bubble will have an image bubble in order to simulate the effects of the wall. In this paper, we will assume that all bubbles in the systems are equally spaced at distance d from the wall, i.e. they are all arranged in a planar fashion a distance d from a solid wall. If their distance of bubble i from bubble j is denoted by $D_{i,j}$, then the matrix form of Eq. (1) can be written as shown in Eq. (3)

VALIDATION OF THE MATHEMATICAL MODEL

To check the validity of the mathematical model, Eq. (2) was solved using the parameter values defined by [4] and compared with the results of the experiment performed by [15], where they studied the behaviour of a single bubble in the absence of an external driving pressure (the value of α was set to zero) near a solid boundary.

The data is taken from Fig. 11 of [15] and Eq. (2) was solved with variable values of $d = 12.0$ mm and $R_0 = 1.2$ mm. The initial conditions used are $R(0) = 4.5$ mm and the initial bubble wall velocity as given by Eq. (4), where $P_{i,0} = 4.64\times10^{-3}P_0$ is the initial pressure inside the bubble and

$$\dot{R}(0) = \frac{1}{\rho c}\left(P_{i,0}-\frac{2\sigma}{R(0)}-P_0\right). \quad (4)$$

Fig. 2 shows the close agreement between the experimental results and the theoretical curve generated by Eq. (2) before the first rebound of the bubble. However, after this first rebound the agreement becomes progressively worse. This is due to the fact that the assumptions that the bubble remains spherical and fixed in space are less valid after the first rebound of the bubble. This will not be an issue for the numerical simulations in the remainder of this study though, because the oscillation of the bubble about its equilibrium radius will be considered, rather than the collapsing-and-rebounding behaviour of the bubble.

Another validation of the model is to compare the solution obtained by solving Eq. (1) with the experimental data obtained by [19]. In this study, they investigated the behaviour of two cavitation bubbles on a wall when subjected to the driving pressure signal shown in Fig 3(a). Utilising the image bubble technique, it will be assumed that each hemispherical bubble on the wall behaves like a spherical bubble, thus Eq. (1) can be used to

$$
\begin{bmatrix}
1 & 0 & 0 & 0 & \cdots & 0 \\
0 & \left(1-\frac{\dot{R}_1}{c}\right)R_1+\frac{4\mu}{\rho c}+\frac{1}{2d}R_1^2 & 0 & \left(\frac{1}{D_{1,2}}+\frac{1}{\sqrt{D_{1,2}+4d^2}}\right)R_2^2 & \cdots & \left(\frac{1}{D_{1,N_{bub}}}+\frac{1}{\sqrt{D_{1,N_{bub}}^2+4d^2}}\right)R_{N_{bub}}^2 \\
0 & 0 & 1 & 0 & \cdots & \vdots \\
0 & \left(\frac{1}{D_{2,1}}+\frac{1}{\sqrt{D_{2,1}^2+4d^2}}\right)R_1^2 & 0 & \ddots & \cdots & \left(\frac{1}{D_{2,N_{bub}}}+\frac{1}{\sqrt{D_{2,N_{bub}}^2+4d^2}}\right)R_{N_{bub}}^2 \\
\vdots & \vdots & \vdots & \vdots & 1 & 0 \\
0 & \left(\frac{1}{D_{N_{bub},1}}+\frac{1}{\sqrt{D_{N_{bub},1}^2+4d^2}}\right)R_1^2 & \cdots & \left(\frac{1}{D_{N_{bub},N_{bub}-1}}+\frac{1}{\sqrt{D_{N_{bub},N_{bub}-1}^2+4d^2}}\right)R_{N_{bub}-1}^2 & 0 & \left(1-\frac{\dot{R}_{N_{bub}}}{c}\right)R_{N_{bub}}+\frac{4\mu}{\rho c}+\frac{1}{2d}R_{N_{bub}}^2
\end{bmatrix}
\begin{bmatrix}
\dot{R}_1 \\ \ddot{R}_1 \\ \vdots \\ \vdots \\ \dot{R}_{N_{bub}} \\ \ddot{R}_{N_{bub}}
\end{bmatrix}
$$

$$
= \begin{bmatrix}
\dot{R}_1 \\
\left[-\frac{\dot{R}_1^2}{2}\left(3-\frac{\dot{R}_1}{c}\right)+\left(1+(1-3\kappa)\frac{\dot{R}_1}{c}\right)\left(\frac{P_0-P_v}{\rho}+\frac{2\sigma}{\rho R_{01}}\right)\left(\frac{R_{01}}{R_1}\right)^{3\kappa}-\frac{2\sigma}{\rho R_1}-\frac{4\mu\dot{R}_1}{\rho R_1}-\right. \\
\left.\left(\frac{1}{d}+\sum_{j\neq i}^{N_{bub}}2\left(\frac{1}{D_{1,j}}+\frac{1}{\sqrt{D_{1,j}^2+4d^2}}\right)\right)R_j\dot{R}_j^2-\left(1+\frac{\dot{R}_1}{c}\right)\frac{P_0-P_v+\alpha\sin(2\pi f_{ext}t)}{\rho}-\frac{2\pi f_{ext}R_a\alpha}{\rho c}\cos(2\pi f_{ext}t)\right] \\
\vdots \\
\dot{R}_{N_{bub}} \\
\left[-\frac{\dot{R}_1^2}{2}\left(3-\frac{\dot{R}_1}{c}\right)+\left(1+(1-3\kappa)\frac{\dot{R}_1}{c}\right)\left(\frac{P_0-P_v}{\rho}+\frac{2\sigma}{\rho R_{0N_{bub}}}\right)\left(\frac{R_{0N_{bub}}}{R_1}\right)^{3\kappa}-\frac{2\sigma}{\rho R_{N_{bub}}}-\frac{4\mu\dot{R}_{N_{bub}}}{\rho R_{N_{bub}}}-\right. \\
\left.\left(\frac{1}{d}+\sum_{j=1}^{N_{bub}-1}2\left(\frac{1}{D_{N_{bub},j}}+\frac{1}{D_{N_{bub},j}^2+4d^2}\right)\right)R_j\dot{R}_j^2-\left(1+\frac{\dot{R}_1}{c}\right)\frac{P_0-P_v+\alpha\sin(2\pi f_{ext}t)}{\rho}-\frac{2\pi f_{ext}R_a\alpha}{\rho c}\cos(2\pi f_{ext}t)\right]
\end{bmatrix}. \quad (3)
$$

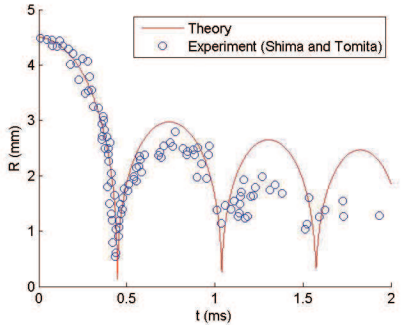

Figure 2: Comparison between numerical and experimental results for the behaviour of a single bubble near a solid boundary in the absence of an external acoustic driving pressure. The solid line is calculated using Eq. (2)

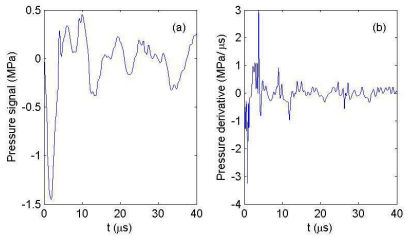

Figure 3: (a) Pressure signal used in the experiment performed by [19] (b) Time derivative of the pressure signal, estimated using a first-order central difference formula

simulate the effects of the wall. However the equation had to be modified to take into account the fact that the external driving pressure signal in the experiment is not sinusoidal, by replacing the $\alpha\sin(2\pi f_{ext}t)$ term with the value of the pressure signal at the specified time, and replacing the $2\pi f_{ext}\cos(2\pi f_{ext}t)$ term with the time derivative of the pressure signal. These values can be obtained from Fig. 3. The modified equation was solved using the parameter values and initial conditions specified in Fig. 3(a) and Fig. 6(a) of [19].

Fig. 4 shows that there is a fairly close relationship between the experimental data and the numerical results. The theoretical curves do predict rebounding of the bubbles after the first collapse, but this is not shown by the experimental data. It is important to note that the experimental data suggests that the maximum value of R is bigger for larger distance between the bubbles, D, and when there are more bubbles in the system. This observation is correctly replicated by the mathematical model. These results suggest that the equations derived in Section 2 based on the Keller-Miksis-Parlitz equation is a reason-

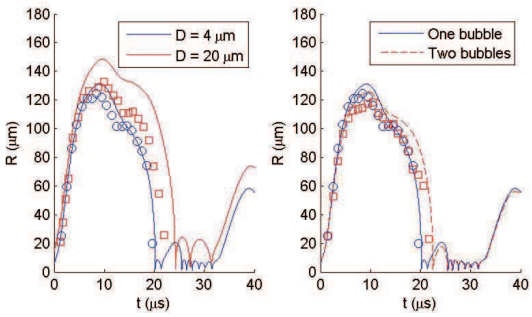

Figure 4: Comparison between numerical results using Eq. (1) and experimental results obtained by [19] for the behaviour of cavitation bubbles on a wall

ably good model of bubble dynamics near a solid boundary.

NUMERICAL SIMULATIONS

To limit this study to a manageable set of parameters, we will assume that the distance between all bubbles in the system, i.e. $D_{ij} = D =$ constant. This means that the distance of any bubble to any other bubble in the bubble population is a constant. For $N_{\text{bub}} = 3$ this situation corresponds to a group of bubbles arranged at the vertices of an equilateral triangle. For this paper, we will only consider cases where all bubbles are arranged on a plane i.e. $N_{\text{bub}} = 1, 2, 3$. If we further assume that at time $t = 0$, all bubbles have the same initial radius and bubble wall velocity is zero, i.e. $R_i(0) = R_0$ and $\dot{R} = 0$, then symmetry will ensure that all bubbles in the system will have the same radius at any instant in time, i.e. $R_i(t) = R_j(t) = R(t)$. Substituting into Eq. (1) with simple algebraic manipulation gives Eq. (5).

Please note that because of all the assumptions that were made, the results presented here would be directly comparable only with experiments in a very specifically designed microfluidic system, rather than experimental data from a group of contrast-agent microbbubles *in vivo*. However, the results may be used as both an ideal reference for a microtechnological application, and to show the possible trends of a contrast-agent system as the number of bubbles is increased from one towards a number that is more typical in medical applications.

In this paper simulations will be carried using typical ultrasound parameters of $\alpha = 40$ kPa and 125kPa and $f_{ext} = 1$ MHz, since these values are commonly used in the literature [7]. The bubbles will start with initial conditions of $R(0) = R_0$ and $\dot{R}(0) = 0$, so that the bubbles oscillate about R_0 due exclusively to the driving pressure. If there is more than one bubble in the group then an inter-bubble distance of $D = 5R_0$ will be used, an arbitrary value used to ensure that the bubbles are close enough to interact but will not collide. Symmetry of the initial conditions will ensure that each and every bubble will exhibit the same behaviour. In this study the behaviour of bubbles that have equilibrium radii, $R_0 = 2$ μm will be analysed, which is much smaller than the bubbles analysed by [6], [7] and [15], and much closer to the size typically used in biomedical applications [1–3].

Our numerical computation typically go through a short transient period and then settle down to a statistically stationary state. Typical time series of the system after the transients have died out is shown in Fig. 5. The data in this figure is computed with one bubble close to the wall with $R_0 = 2\mu$m, $d = 30\mu$m and $f_{ext} = 1/T$=1MHz. The black dots in the figure represent the value of the radius at the end of each period of the external pressure. The value of α is increased from 40 kPa , 125 kPa and 135 kPa and it is clear from Fig. 5 that the response of the system becomes more nonlinear with increasing values of α. For α=40 kPa, the value of R is repeated every period (T seconds) i.e. the system responds with period-1 oscillation. For α=125 kPa, the value of R is repeated every 2 periods ($2T$ seconds) i.e. the system responds with period-2 oscillation. For larger values of $\alpha = 135$ kPa, the response of the system becomes chaotic.

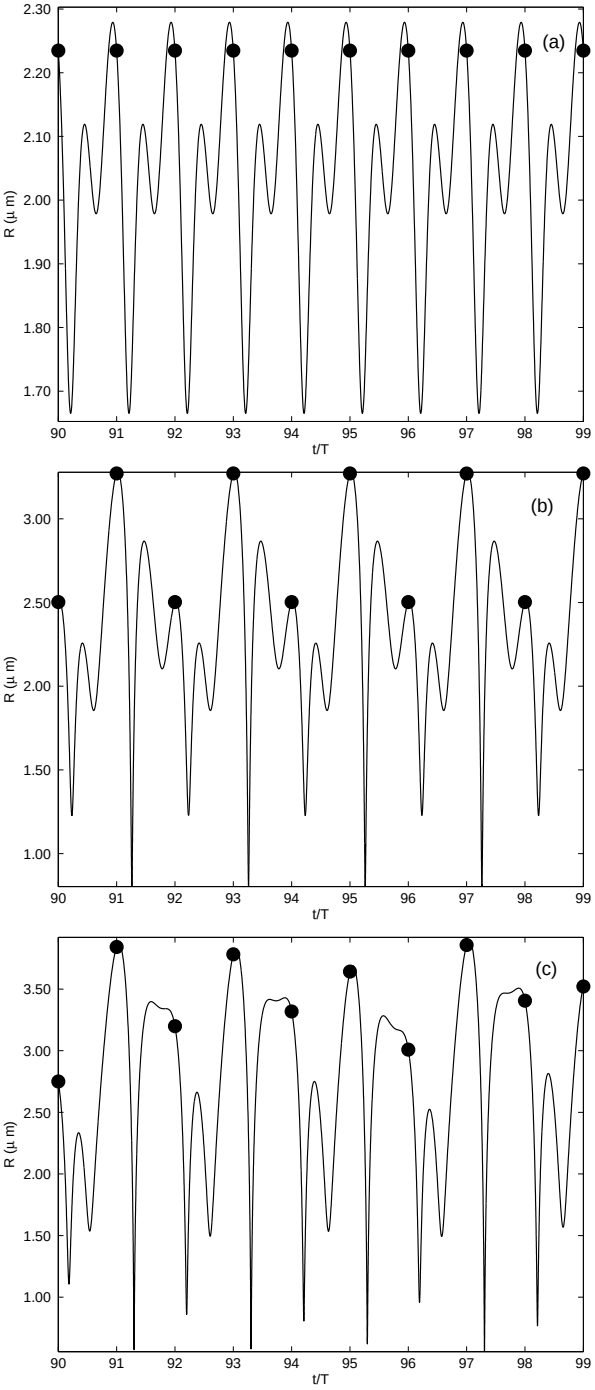

Figure 5: Shows the variation of the radius $R(t)$ of a microbubble with initial radius, $R_0 = 2\mu$m. The bubble is located $d/R_0 = 15$ away from a solid wall. This bubble is forced with a frequency of 1MHz and pressure amplitude of 40 kPa (a), 125 kPa (b) and 135 kPa (c).

Bifurcation characteristics

The information in Fig. 5 can be represented in a bifurcation diagram. Figure 6(d) shows the structure of the bifurcation for a single bubble close to a wall as it transitions from a regular behaviour to chaos as α is incrementally increased. At the end of each driving period, the value of R is recorded and plotted as a function of α (see Fig. 6 (d)). For $\alpha = 40$ kPa, there is only one dominant frequency in the system. Thus, the value of

$$\begin{bmatrix} 1 & 0 \\ 0 & \left(1-\frac{\dot{R}_1}{c}\right)R+\frac{4\mu}{\rho c}+\left(\frac{1}{2d}+\frac{N_{\text{bub}}-1}{D}+\frac{N_{\text{bub}}-1}{\sqrt{D^2+4d^2}}\right)R^2 \end{bmatrix} \frac{d}{dt}\begin{bmatrix} R \\ \dot{R} \end{bmatrix}$$
$$= \begin{bmatrix} \dot{R} \\ \left[-\frac{\dot{R}^2}{2}\left(3-\frac{\dot{R}}{c}\right)-\frac{2\sigma}{\rho R}-\frac{4\mu\dot{R}}{\rho R}+\left(1+(1-3\kappa)\frac{\dot{R}}{c}\right)\left(\frac{P_0-P_v}{\rho}+\frac{2\sigma}{\rho R_0}\right)\left(\frac{R_0}{R}\right)^{3\kappa}-2\left(\frac{N_{\text{bub}}-1}{D}+\frac{N_{\text{bub}}-1}{\sqrt{D^2+4d^2}}\right)R\dot{R}^2-\frac{N_{\text{bub}}}{d}R\dot{R}^2 \right. \\ \left. -\left(1+\frac{\dot{R}}{c}\right)\frac{P_0-P_v+\alpha\sin(2\pi f_{ext}t)}{\rho}-\frac{2\pi f_{ext}R\alpha}{\rho c}\cos(2\pi f_{ext}t)\right] \end{bmatrix} \quad (5)$$

R at the end of every period is the same so all data appear as a single dot in for $\alpha = 40$ kPa in Fig. 6 (d). When the value of α is increased to 125 kPa, the bubble undergoes a period-2 oscillatory motion (i.e. there are two dominant frequencies) and all data appear as a two dots. Then the value of α is increased and the process is repeated. Since the systems behaves in a chaotic fashion for $\alpha = 135$ kPa, all values of R appear as random dots.

By using the normalised radius at every forcing period ($T = 1/f_{ext}$) as the state variable [5; 21] and the driving pressure amplitude as the control parameter [7; 8], bifurcation diagrams were plotted to investigate the chaotic dynamics of the bubble systems considered in this study. Similar to the previous section, a driving frequency of $f_{ext} = 1$ MHz, $R_0 = 2.0$ μm, $D = 5R_0$ (to ensure a large range of pressure amplitudes for which the bubbles do not collide). Bubbles with equilibrium radius are considered here, each bifurcation diagram is plotted for varying distances from $d = 5.0$ μm to $d = 30.0$ μm, and the number of microbubbles in the system is varied from $N_{bub} = 1$ to $N_{bub} = 3$. A single bifurcation diagram is sufficient to describe the characteristics of all bubbles in the group since all bubbles will undergo the same oscillation due to the symmetry of the arrangements initial conditions used in all simulations.

The bifurcation diagrams are only plotted for driving pressure amplitudes at which the bubbles do not collide with the solid boundary, and do not collide with one another. If either of these occur, then clearly the assumption that the bubbles remain spherical is no longer valid, so the solution must be discarded. In the cases considered the maximum pressure amplitude that provides a physically sensible solution lies between $\alpha = 124$ kPa and $\alpha = 138$ kPa, which is determined on a case-by-case basis.

For a single bubble a distance $d = 2.5R_0$ from a solid boundary, Fig. 6(a) shows a period-1 solution up to the period-doubling bifurcation occuring at $\alpha \approx 110$ kPa. This period-2 solution extends up to $\alpha \approx 125$ kPa, where, at this upper limit of the pressure amplitude, another period-doubling bifurcation occurs to form a period-4 solution.

Fig. 6(b) shows that when the distance from the solid boundary is increased to $d = 5R_0$ the bubble undergoes period-1 oscillations up to a period-doubling bifurcation at $\alpha \approx 120$ kPa, which is greater than in the previous case. The resulting period-2 solution then extends up to another period-doubling bifurcation at $\alpha \approx 130$ kPa. After a small increase in pressure amplitude, the period-4 solution splits into a series of points arranged vertically on top of one another, which indicates chaotic oscillations of the microbubble for these pressure amplitudes.

If the distance from the solid boundary is increased to $d = 10R_0$, Fig. 6(c) shows that the bubble undergoes period-1 osillations up to a period-doubling bifurcation at $\alpha \approx 120$ kPa. The period-2 solution extends up to $\alpha \approx 130$ kPa, when the system begins to lead into a state of full chaos. A similar route to chaos is shown in Fig. 6(d), which shows that when the distance from the solid boundary is increased to $d = 15R_0$, the bubble undergoes period-1 oscillations, as before, up to a period-doubling bifurcation at $\alpha \approx 125$ kPa. The resulting period-2 solution then begins to make its transition to chaos at $\alpha \approx 135$ kPa.

Comparing all four plots in Fig. 6, it can be observed that the microbubble exhibits very similar routes to chaos for all distances considered. But, as the distance between the bubble and the solid boundary is increased, the system begins its bifurcations and route to chaos at a higher driving pressure amplitude.

When a second microbubble is added to the bubble system, it exhibits very different bifurcation characteristics. This is consistent with the results of [7] and [8] who showed that adding a bubble to an existing bubble cluster can significantly alter the bifurcation characteristics of the system. Fig. 7(a) shows that for two bubbles located a distance $d = 2.5R_0$ from a solid boundary, the bubbles undergo period-1 oscillations up to $\alpha \approx$ 125 kPa, when the system makes a transition directly to chaos. In our simulations, we did not observe any period-2 oscillations.

One the other hand, when the distance between the bubbles and the boundary is increased, the bubbles do not exhibit any chaotic dynamics. For a distance of $d = 5R_0$, Fig.7(b) shows a period-1 solution up to a period-doubling bifurcation at $\alpha \approx$ 100 kPa, after which the branches of the period-2 solution gradually converge back to a period-1 solution. Similar behaviour is observed for larger distances, although the solution does not quite revert back to a period-1 solution within the considered range of pressure amplitudes, and the bifurcation occurs at a higher pressure amplitudes — from Fig. 7(c), when $d = 20.0$ μm the bifurcation occurs at $\alpha \approx 105$ kPa, while from Fig. 7(d), when $d = 30.0$ μm the bifurcation occurs at $\alpha \approx 110$ kPa. So for larger distances from the solid boundary, the bubbles actually remain in a state of order at higher pressure amplitudes, unlike when the bubbles are close to the boundary, in which case they exhibit chaotic dynamics.

Adding a third microbubble to the system again significantly alters its bifurcation properties. Fig. 8(a) shows that when the distance from the bubbles to the solid boundary is $d = 2.5R_0$, the system makes a sudden transition from a period-1 solution to a chaotic solution at $\alpha \approx 95$ kPa. As was the case in the two-bubble scenario, when the distance from the boundary is increased, the bubbles exhibit a more orderly behaviour. When $d = 5R_0$, Fig. 8(b) shows that the bubbles undergo period-1 oscillations up to a period-4 bifurcation at $\alpha \approx 115$ kPa. Fig. 8(c) shows similar behaviour at $d = 10R_0$ with the bifurcation occurring at the higher pressure amplitude of $\alpha \approx 125$ kPa. From Fig. 8(d), at $d = 15R_0$ bifurcation occurs when $\alpha \approx 130$ kPa. So, just as in the two-bubble case, the bubbles remain in a state of order at higher pressure amplitudes when the distance between the bubbles and the solid boundary is relatively large, but when this distance is small then the bubbles exhibit chaotic dynamics.

Maximum Radius

Another way of looking at the effects of the wall is to plot the maximum extension of the radius of a bubble versus the normalized distance d/R_0 from the solid boundary. This is important because there are recent research activities that use microbubbles to enable transportation of drugs to a target site in

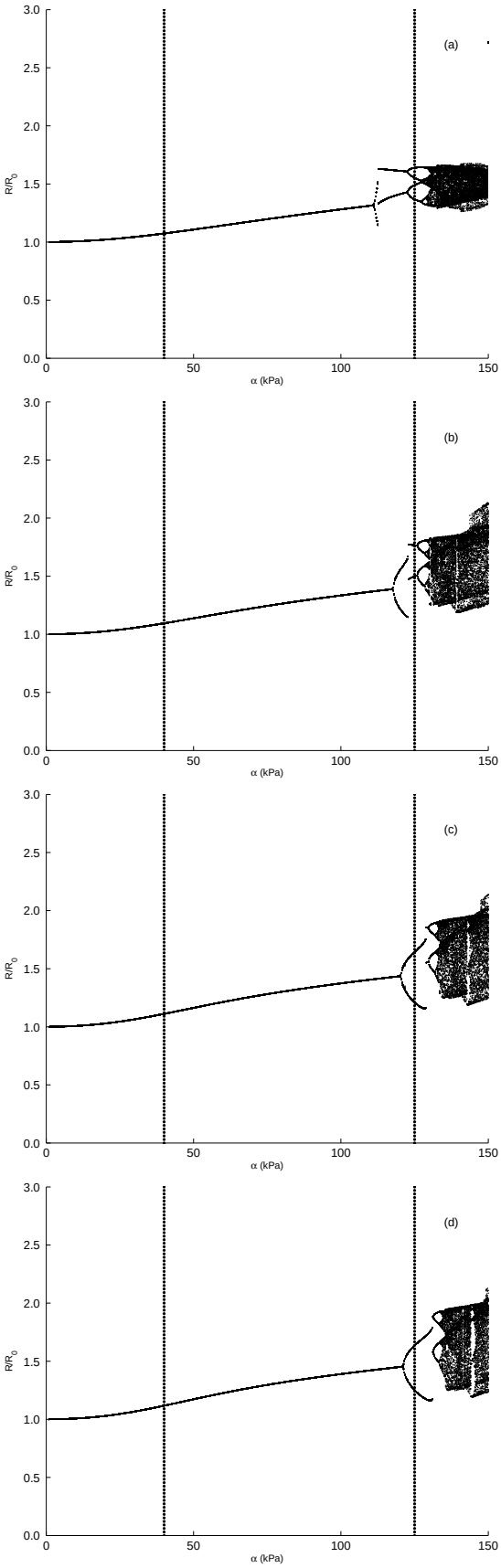

Figure 6: Bifurcation characteristics for a single bubble near a solid boundary with $R_0 = 2.0$ μm (a) $d/R_0 = 2.5$, (b) $d/R_0 = 5.0$, (c) $d/R_0 = 10.0$, (d) $d/R_0 = 15.0$. The two vertical lines in the figure shows reference location where $\alpha = 40$ and $\alpha = 125$.

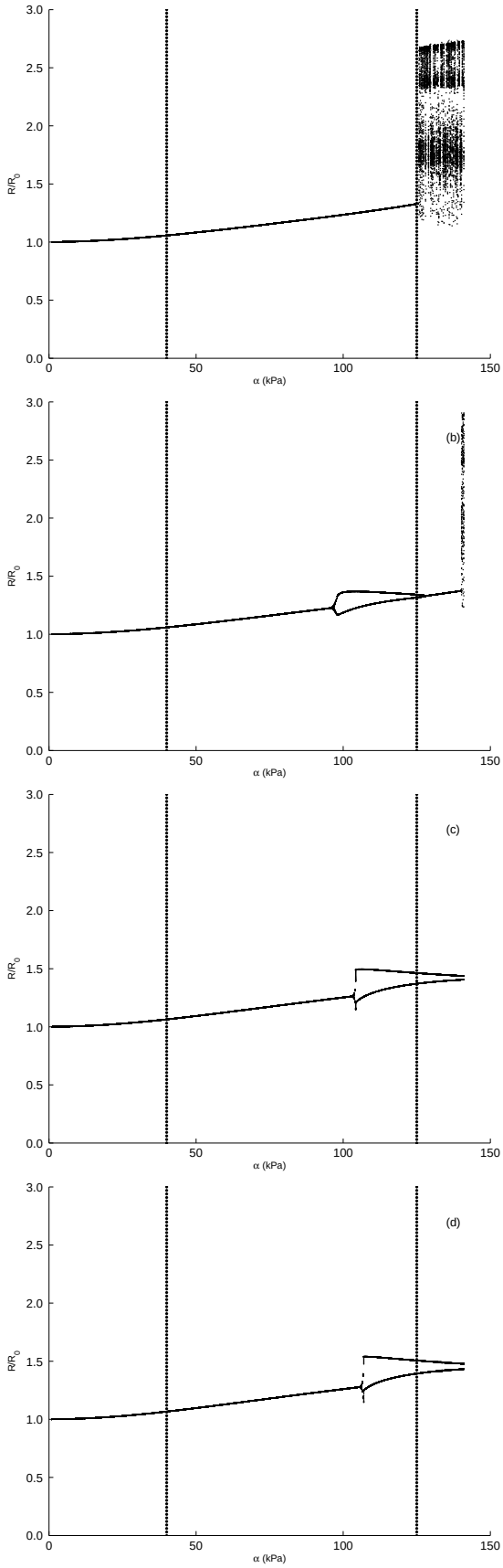

Figure 7: Bifurcation characteristics for two bubbles near a solid boundary with $R_0 = 2.0$ μm (a) $d/R_0 = 2.5$, (b) $d/R_0 = 5.0$, (c) $d/R_0 = 10.0$, (d) $d/R_0 = 15.0$. The two vertical lines in the figure shows reference location where $\alpha = 40$ and $\alpha = 125$.

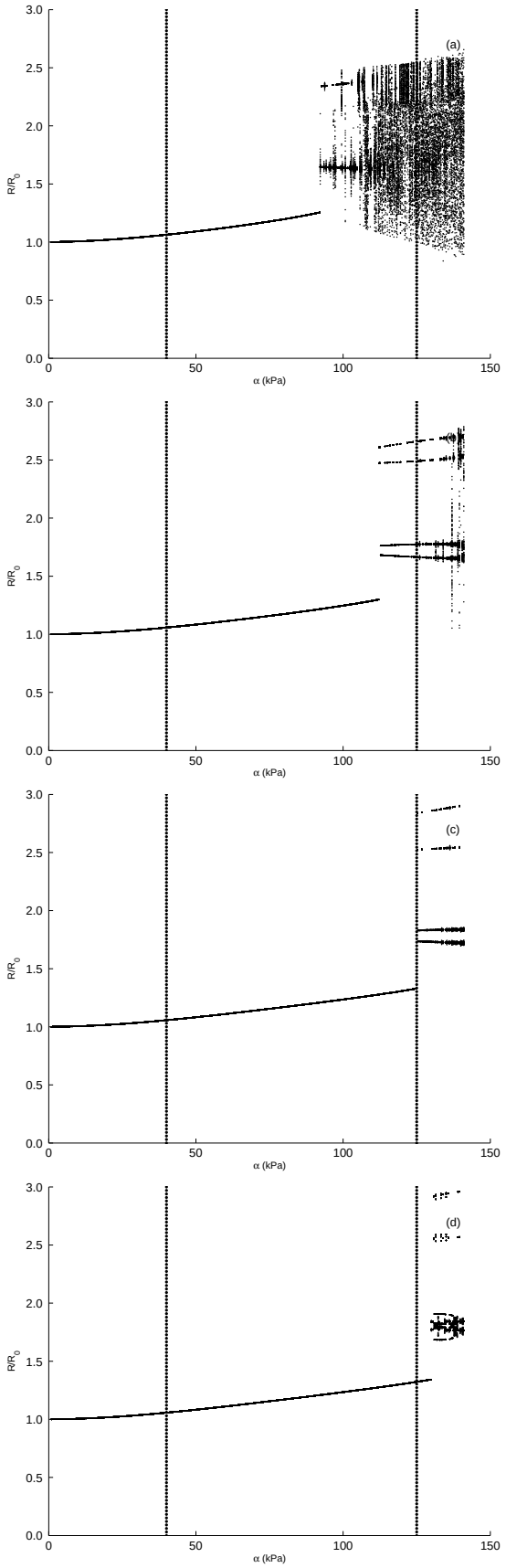

Figure 8: Bifurcation characteristics for three bubbles near a solid boundary with $R_0 = 2.0$ μm (a) $d/R_0 = 2.5$, (b) $d/R_0 = 5.0$, (c) $d/R_0 = 10.0$, (d) $d/R_0 = 15.0$. The two vertical lines in the figure shows reference location where $\alpha = 40$ and $\alpha = 125$.

the body. For such application, the methodology requires identification of physical parameters that will give rise to large bubble oscillations, leading to bubble rupture and localised drug delivery. The bifurcation diagrams computed thus far only gives information on the frequency content of the bubble response. Figure 9 shows

$$\varepsilon = \frac{R_{max}}{R_0} \tag{6}$$

computed with data for different values of d/R_0, and provides a clearer idea of the effect of the distance from the solid boundary on amplitude of bubble oscillation. Each graph is plotted from the minimum distance before the bubble collides with the solid boundary during its motion up to $d/R_0 = 15$. Simulations were conducted with $\alpha = 40$ kPa and $\alpha = 125$ kPa and the dynamics of the bubble oscillations is indicated by the vertical lines in Figs. 6-8. For $\alpha = 40$ kPa bubble response is dominated by one frequency for $N_{bub} = 1, 2$ and 3. $\alpha = 125$ kPa will generate a response that has 1, 2 or many frequencies, depending on the number of bubbles and distance from the walls.

It can be observed from Fig. 9(a) that for $\alpha = 40$ kPa and $N_{bub} = 2, 3$, ε increases as the bubbles approach the boundary. For $N_{bub} = 1$ the opposite is true with the value of ε increasing with d. There appears to be no clear trend in the data on how R_{max} changes with d and the number of bubbles in the system. However, the differences are very small. The variation in R_{max} is only about 3%-4% for all the simulations reported here. It is clear that the wall has a negligible effect on the bubble response for $\alpha = 40$ kPa.

The bubble response for $\alpha = 125$ kPa is shown in Fig. 9(b). For this case, the effects of d on R_{max} is much more significant. For $N_{bub} = 1$ the data in this figure shows that R_{max} increases with d up to a $d/R_0 \approx 6 - 7$ and then there appears to be a sudden drop in the value of R_{max} followed by a more gradual decrease of R_{max} with d. The data in Fig. 9(b) should be compared with the corresponding data in Fig. 6. As we move the bubbles away from the wall, the number of dominant frequencies in the system is 4 for $d/R_0 = 2.5$, 2-4 for $d/R_0 = 5.0$ and 2 for $d/R_0 = 10.0$ and 15.0. The sudden decrease in R_{max} appear to correspond to the change of number of dominant frequencies from 4 to 2. The R_{max} values for $N_{bub} = 2$ appear to be lower than the R_{max} values for $N_{bub} = 1$. Figure 7 shows that the number of dominant frequencies in the bubble response for $N_{bub} = 2$ and $\alpha = 125$ is only 1-2. Comparing the data for $N_{bub} = 1$ and 2 so far seems to suggest that R_{max} will increase with the number of dominant frequencies in the bubble response. This is confirmed with Fig. 8 which shows that for $N_{bub} = 3$, the bubble oscillations undergoes chaotic behaviour for $d/R_0 = 2.5$, less chaotic for $d/R_0 = 5.0$ and only one dominant frequency for $d/R_0 = 10$ and 15. Fig. 9(b) shows that the corresponding values of R_{max} appear to be large up till about $d/R_0 = 10$ and drops quite suddenly for $d/R_0 > 10$.

CONCLUSION

In this study, a mathematical model is derived that can be used to simulate the dynamics of a group of bubbles in the vicinity of a solid wall. This model is based on the Keller-Miksis-Parlitz equation with coupling terms that describe the effects of nearby bubbles and the solid boundary. These equations were verified by comparison with available experimental experimental data. In order to limit the number of parameters involved in this problem, the study is limited to bubble arrangements where all bubbles are equally spaced from each other and all bubbles are equally spaced from the solid wall. Thus, the num-

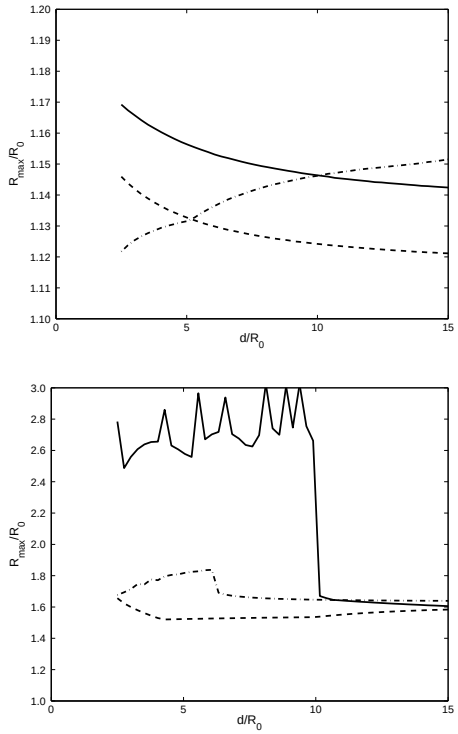

Figure 9: Effect of distance from the solid boundary for (a) $\alpha = 40$kPa, (b) $\alpha = 125$kPa. —·— $N_{bub} = 1$, – – – – $N_{bub} = 2$, ——— $N_{bub} = 3$.

ber of bubbles in this study is limited to 1, 2 or 3. Numerous numerical simulations were performed to investigate the effect of the solid boundary on the oscillations of the microbubbles for ultrasound parameters.

The bifurcation diagrams of the bubble systems shows that the solid boundary does have a significant effect on the bifurcation structure of microbubbles oscillations. When the distance between the microbubbles and the solid boundary is decreased, a bubble system is more likely to exhibit chaotic dynamics, while the system also makes the transition from order to chaos at lower driving pressure amplitudes. It was also found that the solid boundary has an effect on the amplitude of oscillation of the microbubbles. In general, the amplitude of oscillation, R_{max}, increases with the pressure forcing amplitude, α. Larger values of α give rise to larger values of R_{max}. For a given value of α, the value of R_{max} appear to have a positive correlation with the number of dominant frequencies in the bubble response. Bubble systems with 1-2 dominant frequencies appear to have smaller values of R_{max} when compared with microbubble systems which undergoes chaotic oscillations.

REFERENCES

[1] M. Blomely, J. Cooke, E. Unger, M. Monaghan, and D. Cosgrove, "Microbubble contrast agents: a new era in ultrasound," *British Medical Journal*, vol. 322, pp. 1222–1225, 2001.

[2] C. Coussios and R. Roy, "Applications of acoustics and cavitation to noninvasive therapy and drug delivery," *Annual Review of Fluid Mechanics*, vol. 40, pp. 395–420, 2008.

[3] M. Postema and O. Gilja, "Ultrasound-directed drug delivery," *Current Pharmaceutical Biotechnology*, vol. 8, pp. 355–361, 2007.

[4] J. Keller and M. Miksi, "Bubble oscillations of large amplitude," *The Journal of the Acoustical Society of America*, vol. 68, pp. 628–633, 1980.

[5] U. Parlitz, V. Englisch, C. Scheffczyk, and W. Lauterborn, "Bifurcation structure of bubble oscillators," *The Journal of the Acoustical Society of America*, vol. 88, pp. 1061–1077, 1990.

[6] A. Ooi and R. Manasseh, "Coupled nonlinear oscillations of microbubbles," *Australian & New Zealand Industrial and Applied Mathematics Journal*, vol. 46E, pp. C102–C116, 2005.

[7] K. Chong, C. Quek, F. Dzaharudin, A. Ooi, and R. Manasseh, "The effects of coupling and bubble size on the dynamical-systems behaviour of a small cluster of microbubbles," *Journal of Sound and Vibration*, vol. 329, pp. 687–699, 2010.

[8] C. MacDonald and J. Gomatam, "Chaotic dynamics of microbubbles in ultrasonic fields," *J. Mechanical Engineering Science Proc. IMechE*, vol. 220, 2006.

[9] E. Payne, S. Illesinghe, A. Ooi, and R. Manasseh, "Symmetric mode resonance of bubbles attached to a rigid boundary," *J Acoust Soc Am*, vol. 118, p. 2841, 2005.

[10] S. Illesinghe, A. Ooi, and R. Manasseh, "Eigenmodal resonances of polydisperse bubble systems on a rigid boundary," *J. Acoust. Soc. Am*, vol. 126, pp. 2929–2938, Dec 2009.

[11] J. Blake and D. Gibson, "Growth and collapse of a vapour cavity near a free surface," *Journal of Fluid Mechanics*, vol. 111, pp. 123–140, 1981.

[12] J. Isselin, A. Alloncle, and M. Autric, "n laser induced single bubble near a solid boundary: Contribution to the understanding of erosion phenomena," *Journal of Applied Physics*, vol. 84, pp. 5766–5771, 1998.

[13] W. Lauterborn and H. Bolle, "xperimental investigations of cavitation-bubble collapse in the neighbourhood of a solid boundary," *ournal of Fluid Mechanics*, vol. 72, pp. 391–399, 1975.

[14] M. Plesset and R. Chapman, "Collapse of an initially spherical vapour cavity in the neighbourhood of a solid boundary," *Journal of Fluid Mechanics*, vol. 47, pp. 283–290, 1971.

[15] A. Shima and Y. Tomita, "The behaviour of a spherical bubble near a solid wall in a compressible liquid," *Ingenieur-Archiv*, vol. 51, pp. 243–255, 1981.

[16] A. Shima and T. Fujiwara, "The behaviour of two bubbles near a solid wall," *Archive of Applied Mechanics*, vol. 62, pp. 53–61, 1992.

[17] W. Lauterborn and A. Koch, "Holographic observation of period-doubled and chaotic bubble oscillations in acoustic cavitation," *Physical Review A*, vol. 35, pp. 1975–1993.

[18] R. Mettin, I. Akhatov, U. Parlitz, C. Ohl, and W. Lauterborn, "Bjerknes forces between small cavitation bubbles in a strong acoustic field," *Physical Review E*, vol. 56, pp. 2924–2931, 1997.

[19] N. Bremond, M. Arora, S. Dammer, and D. Lohse, "Interaction of cavitiation bubbles on a wall," *Physics of Fluids*, vol. 18, p. 121505, 2006.

[20] E. Klaseboer and B. Khoo, "A modified rayleigh-plesset model for a non-spherically symmetric oscillating bubble with applications to boundary integral methods," *Engineering Analysis with Boundary Elements*, vol. 30, pp. 59–71, 2006.

[21] W. Lauterborn and U. Parlitz, "Methods of chaos physics and their application to acoustics," *The Journal of the Acoustical Society of America*, vol. 84, pp. 1975–1993, 1988.